2014

Relative Contributions of Ocean Mass and Deep Steric Changes to Sea Level Rise Between 1993 and 2013

Sarah G. Purkey
University of Washington

Gregory C. Johnson
University of Washington

Don P. Chambers
University of South Florida, donc@usf.edu

AGU PUBLICATIONS

JGR

Journal of Geophysical Research: Oceans

RESEARCH ARTICLE

10.1002/2014JC010180

Relative contributions of ocean mass and deep steric changes to sea level rise between 1993 and 2013

Sarah G. Purkey[1,2], Gregory C. Johnson[1,2], and Don P. Chambers[3]

[1]School of Oceanography, University of Washington, Seattle, Washington, USA, [2]NOAA/Pacific Marine Environmental Laboratory, Seattle, Washington, USA, [3]College of Marine Sciences, University of South Florida, St. Petersburg, Florida, USA

Key Points:
- Regional and global mass addition estimates from sea level and steric data
- Regional and global mass addition estimates from GRACE compare well
- Full-depth steric measurements yield deep ocean contribution to sea level rise

Correspondence to:
G. C. Johnson,
gregory.c.johnson@noaa.gov

Citation:
Purkey, S. G., G. C. Johnson, and D. P. Chambers (2014), Relative contributions of ocean mass and deep steric changes to sea level rise between 1993 and 2013, *J. Geophys. Res. Oceans*, *119*, 7509–7522, doi:10.1002/2014JC010180.

Received 20 MAY 2014
Accepted 7 OCT 2014
Accepted article online 10 OCT 2014
Published online 7 NOV 2014

Abstract Regional and global trends of Sea Level Rise (SLR) owing to mass addition centered between 1996 and 2006 are assessed through a full-depth SLR budget using full-depth in situ ocean data and satellite altimetry. These rates are compared to regional and global trends in ocean mass addition estimated directly using data from the Gravity Recovery and Climate Experiment (GRACE) from 2003 to 2013. Despite the two independent methods covering different time periods with differing spatial and temporal resolution, they both capture the same large-scale mass addition trend patterns including higher rates of mass addition in the North Pacific, South Atlantic, and the Indo-Atlantic sector of the Southern Ocean, and lower mass addition trends in the Indian, North Atlantic, South Pacific, and the Pacific sector of the Southern Ocean. The global mean trend of ocean mass addition is 1.5 ($\pm$0.4) mm yr^{-1} for 1996–2006 from the residual method and the same for 2003–2013 from the GRACE method. Furthermore, the residual method is used to evaluate the error introduced into the mass budget if the deep steric contributions below 700, 1000, 2000, 3000, and 4000 m are neglected, revealing errors of 65%, 38%, 13%, 8%, and 4% respectively. The two methods no longer agree within error bars when only the steric contribution shallower than 1000 m is considered.

1. Introduction

Global mean sea level has risen at a rate of 3.2 ($\pm$0.4) mm yr^{-1} from 1993 to 2010, reflecting the sum of steric expansion from anthropogenic warming and increased ocean mass from changes in land-ocean water balance [e.g., *Leuliette et al.*, 2004; *Ablain et al.*, 2009; *Church and White*, 2011; *Church et al.*, 2013]. However, Sea Level Rise (SLR) is not uniform, with some coastal communities experiencing rates 3 times the global average, while other locations have seen little rise over this time period [e.g., *Nerem et al.*, 2010; *Church et al.*, 2013; *Stammer et al.*, 2013]. A better understanding of the past trends in total SLR and the contributions from mass addition and steric expansion is needed in order to predict accurately future local and global SLR.

Steric expansion is estimated globally to be adding 1.1 ($\pm$0.3) mm yr^{-1} to SLR from 1993 to 2010 [e.g., *Cazenave et al.*, 2009; *Church et al.*, 2011, 2013; *Levitus et al.*, 2012; *Rhein et al.*, 2013]. In the global mean, most of the steric contribution is from anthropogenic warming, with freshening having little net effect [*Lowe and Gregory*, 2006]. The upper ocean has expanded the fastest, with warming between the surface and 700 m contributing an estimated 0.7 mm yr^{-1} from 1993 to 2008 to global SLR, and the portion between 700 and 3000 m contributing an additional $\sim$0.1 mm yr^{-1} [e.g., *Church et al.*, 2011, 2013]. Below 3000 m, the deep ocean is occupied by two water masses exhibiting different steric trends. North Atlantic Deep Water, formed through open water deep convection in the North Atlantic [*LeBel et al.*, 2008], has shown multidecadal oscillations with a slightly cooling trend since the mid-1970s [e.g., *Mauritzen et al.*, 2012]. Meanwhile, Antarctic Bottom Water, formed by dense plumes cascading down certain portions of the Antarctic continental slope [*Orsi et al.*, 1999], has warmed between the 1990s and 2000s, contributing an additional 0.11 ($\pm$0.10) mm yr^{-1} to global SLR rates [*Purkey and Johnson*, 2010].

Global mean sea level changes owing to increases in ocean mass can be monitored directly from changes in Ocean Bottom Pressure (OBP) or from the sum in changes of land storage, through monitoring of glacial retreat, melting polar ice sheets, and changes in terrestrial water storage. Global OBP changes, estimated from small fluctuations in Earth's gravitational field by the Gravity Recovery and Climate Experiment (GRACE) twin satellites, suggest an increase in global ocean mass at a rate of 1.8 ($\pm$0.5) mm yr^{-1} from 2003

to 2012, accounting for both internal variability and uncertainty in the Glacial Isostatic Adjustment (GIA) [*Chambers*, 2009; *Chambers et al*., 2010; *Johnson and Chambers*, 2013]. This result is in good agreement with estimates in changes in land freshwater storage owing to glacier retreat, polar ice sheets loss, and anthropogenic freshwater storage of 1.66 ($\pm$0.73) mm yr^{-1} between 1993 and 2008, despite the difference in time periods [*Church et al*., 2013].

Since the start of GRACE in 2003, agreement between global mean total sea level and the sum of steric and mass contributions has progressively improved while error bars have shrunk [e.g., *Lombard et al*., 2005; *Domingues et al*., 2008; *Willis et al*., 2008; *Ablain et al*., 2009; *Cazenave et al*., 2009; *Leuliette and Miller*, 2009; *Chambers and Willis*, 2010; *Leuliette and Willis*, 2011; *Rhein et al*., 2013]. These advances have come from improvements in understanding of the GIA as well as instrumentation biases and errors [e.g., *Willis et al*., 2008; *Leuliette and Miller*, 2009; *Chambers and Bonin*, 2012].

Local SLR trends can vary dramatically from the global mean, owing to both steric and mass spatial variability [e.g., *Merrifield et al*., 2012; *Johnson and Chambers*, 2013; *Stammer et al*., 2013]. Local total sea level trends are mostly associated with steric variations reflecting redistribution of heat and salt within the ocean [e.g., *Fukumori and Wang*, 2013; *Stammer et al*., 2013]. However, the ocean mass distribution also varies temporally and spatially, albeit with smaller magnitudes [*Johnson and Chambers*, 2013]. Any addition in ocean mass from changes in freshwater storage between ocean and land will redistribute uniformly throughout the global oceans within days [*Lorbacher et al*., 2012]. However, local deviations from this global mean ocean mass trend can be driven by a barotropic circulation response to changes in wind stress curl [e.g., *Chambers and Willis*, 2008], changes in Earth's gravitational or rotational field from mass redistributions such as melting ice sheets flowing into the ocean [*Bamber and Riva*, 2010], or local GIA effects. Unlike steric changes that fluctuate on relatively small spatial scales, ocean mass varies on large, slow, basin-wide scales [*Johnson and Chambers*, 2013].

Here we present regional and global trends in the rate of ocean mass addition using two independent methods. First, we estimate average mass trends centered between 1996 and 2006 within seven geographical ocean regions using the residual between steric sea level (SSL) from repeated full-depth in situ temperature and salinity data and total sea surface height (SSH) from satellite altimetry, hereafter *the residual method* (section 3). Second, we estimate regional and global trends in ocean mass measured by the GRACE twin satellites from 2003 to 2013 for comparison, hereafter *the GRACE method* (section 4). We then compare the findings from both methods (section 5). Furthermore, we use the residual method to provide direct estimates of the relative contributions of the subsurface ocean regionally and globally from the surface to 300, 700, 1000, 2000, 3000, 4000, and 6000 m, estimating biases introduced into SLR budgets by excluding steric changes below these different depths (section 6). We conclude with a discussion and summary (section 7).

2. Data

We use four global data products to compute the ocean mass component of sea level in seven regions and globally. The residual method uses in situ full-depth ship-based oceanographic data (section 2.1), mapped AVISO satellite altimetry (section 2.2), and mapped monthly OBP from GRACE (section 2.3) to calculate decadal ocean mass trends from the residual between total sea level and SSL trends, accounting for average seasonal mass redistributions. The GRACE method calculates ocean mass trends from regional monthly time series of OBP produced using averaging kernels (section 2.4).

2.1. In Situ Full-Depth Oceanographic Data

SSL is computed using full-depth, high-quality, conductivity-temperature-depth (CTD) profiles collected nominally every 55 km along ocean sections occupied 2 or more times between October 1992 and 2013 (Figures 1 and 2). Since the end of the World Ocean Circulation Experiment (WOCE) around the turn of the century, these occupations are collected as part of the international Global Ocean Ship-based Hydrographic Investigation Program (GO-SHIP).

A full description of the data quality and intercruise salinity adjustments is given in *Purkey and Johnson* [2013], and only two differences apply here. First, in this study we only use data collected after the start of AVISO altimetry mapped products in October of 1992 (Figure 2). The elimination of the earlier occupations

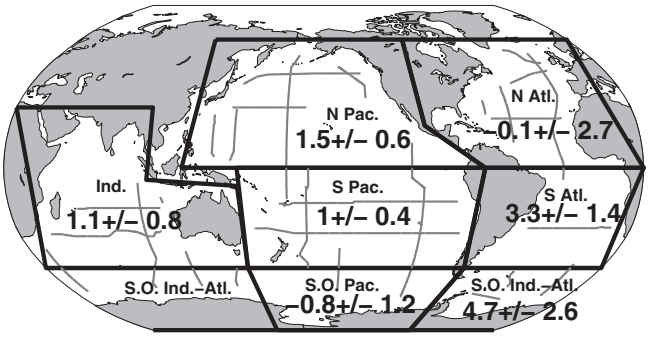

Figure 1. Boundaries (black lines) of study regions termed North Pacific (N. Pac.), North Atlantic (N. Alt.), Indian (Ind.), South Pacific (S. Pac.), South Atlantic (S. Atl.), Indian–Atlantic sector of the Southern Ocean (S.O. Ind.-Atl.), and the Pacific sector of the Southern Ocean (S.O. Pac.) with mean ocean mass sea level rise (mm yr^{-1}) calculated from the residual between total and SSL changes along sections (gray lines). Uncertainties given are two-tailed 90% confidence limits.

reduces data coverage, most notably: the 0°E section and the southern part of the ~25°W section in the Atlantic, the 24°N and the northern end of the 150°W section across the Pacific, and the 67°S section across the Pacific sector of the Southern Ocean (Figure 1). Second, we do not combine sections if occupied multiple times in a single year for this analysis because of large seasonal signals in the upper water column.

The 27 remaining repeated sections provide broad spatial coverage of most of the global ocean, with the exception of the northwest Indian, north east Pacific and south Atlantic oceans (Figure 1). Here we assume the mean of the along-section residuals are representative of the regional means and variability. We discuss this assumption and areas where limited data may bias our results further in section 7.

2.2. SSH From AVISO

The total changes in SSH between section occupations are estimated using the SsaltoDuacs multimission delayed time high-resolution global-merged mapped sea level anomaly (MSLA; e.g., Figure 3a). The mapped products combine altimetry measurements from the Jason, Envisat, GFO, ERS-2, and TOPEX/Poseidon satellites [*Ducet et al*., 2000]. The MSLA provides mapped SSH anomalies on a 1/3° × 1/3° Mercator grid with a weekly temporal resolution between October 1992 and May 2013. Here we consider uncertainties from formal SSH mapping errors, regional variability, and the GIA correction for changes in the sea floor height [*von Schuckmann et al*., 2014] in the error analysis.

2.3. Mapped Ocean Bottom Pressure From GRACE

We estimate seasonal mass fluctuations between repeat occupations of sections during varying times of the year using 10 years of gridded monthly maps of OBP GRACE release 05 [*Chambers and Bonin*, 2012]. The spherical harmonic coefficients from the GRACE gravity field are used to produce monthly 1° × 1° resolution global ocean maps in equivalent water thickness anomalies. As of May 2013, monthly maps were available from January 2003 through January 2013 with only 6 months missing. The maps are smoothed with a 500 km horizontal Gaussian smoother. Postglacial rebound and antistripping corrections have been applied. In addition, we apply a 300 km land mask to avoid land leakage biases and remove the average atmospheric pressure loading signal from European Center for Medium Range Weather Forecasts [*Flechtner*, 2007]. Here we compare data products from all three of the GRACE processing centers; Center for Space Research (CSR), the Helmholtz Centre Potsdam, German Research Center for Geosciences (GFZ), and the Jet Propulsion Laboratory (JPL). All results presented hereafter are from CSR, with any differences among the products noted. The uncertainty on the mapped OBP is estimated to be 1 cm of equivalent water thickness anomaly throughout most of the ocean with slightly higher uncertainties of 1–2 cm in the polar regions [*Chambers and Bonin*, 2012].

2.4. Regional Average Ocean Bottom Pressure

While mapped GRACE data are useful for investigating spatial patterns of variability, the applied 500 km smoother and destriping greatly damp the magnitude of variation in OPB and bias long-term trends [*Johnson and Chambers*, 2013]. Hence, we estimate regional decadal trends in ocean mass directly from the spherical harmonic coefficients of the GRACE gravity field using an averaging kernel for each of the seven regions (Figure 1). These averaging kernels are used to produce a monthly mean water thickness anomaly for each of the seven regions following the procedure described in *Chambers* [2009]. Even these regional averaging kernels are likely to underestimate the trends slightly. GIA corrections are applied to all the

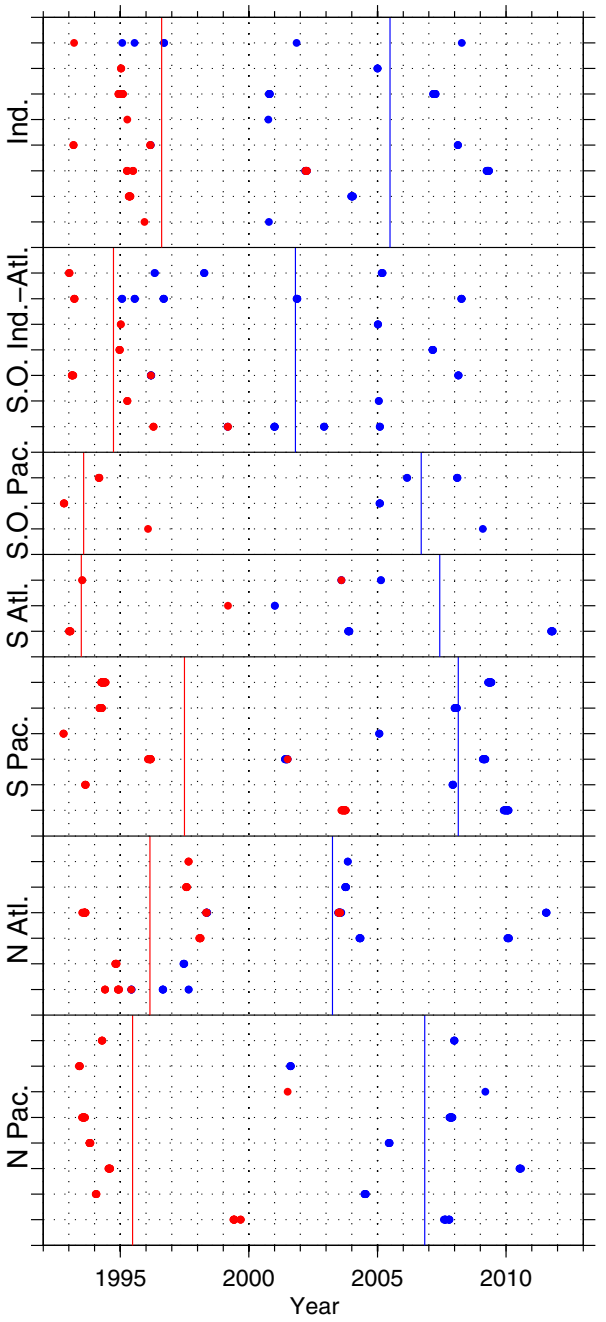

Figure 2. Date of first (red) and subsequent (blue) occupations of all sections within each region boundary (Figure 1) with distance-weighted regional means (vertical lines) of first (red) and subsequent (blue) occupations showing the average time period captured by each regional trend (Table 1).

GRACE time series. The GIA correction uncertainty is $\pm$0.3–0.6 mm yr^{-1}, depending on the region, for all trends calculated using the GRACE data here [*Chambers et al.*, 2010]. In addition, the monthly global atmospheric pressure fluctuations are removed. The monthly standard errors for each regional time series range from 0.6 to 2.7 cm of equivalent water thickness. The standard errors scale inversely with the size of the region.

3. Ocean Mass Trends From Residuals

To find the changes in mass, we calculate the residual between changes in SSH and full-depth SSL along repeats of hydrographic lines. Once the steric component is removed, the residuals along sections include changes in local mass owing to both long-term trends and mass redistribution associated with large-scale seasonal shifts in ocean circulation [e.g., *Johnson and Chambers*, 2013]. Therefore, we also apply a correction for the expected seasonal mass redistribution estimated from the 10 year GRACE global mapped OBP time series. After the seasonal mass redistribution is accounted for, the residual will be the trend in local mass plus some remaining noise. We take large regional means using all residuals within a region boundary to reduce the noise and find statistically significant estimates of the mean regional mass trends. This method works as well as it does because local mass imbalances adjust globally over time scales of days via surface gravity waves [e.g., *Lorbacher et al.*, 2012].

We divide the ocean into seven regions to capture some of the expected large-scale variation in mass addition rates [*Johnson and Chambers*, 2013] while still ensuring we have enough data within a region to get a reliable mean (Figure 1). Based on this previous work, we divide the Atlantic, Pacific, and Indian oceans into North (60°N to the equator), South (equator to 50°S), and Southern Ocean (south of 50°S). We consider the Indian and Atlantic sectors of the Southern Ocean as one region because mass trends over our study period in these two regions have been similar, perhaps owing to changes in the Weddell Gyre affecting both regions [*Johnson and Chambers*, 2013]. We also combine the south and north Indian Ocean into one region. We have no full-depth repeat sections in the Arctic Ocean, and the sea ice there would make it difficult to use altimeter data, therefore it is not included in this study.

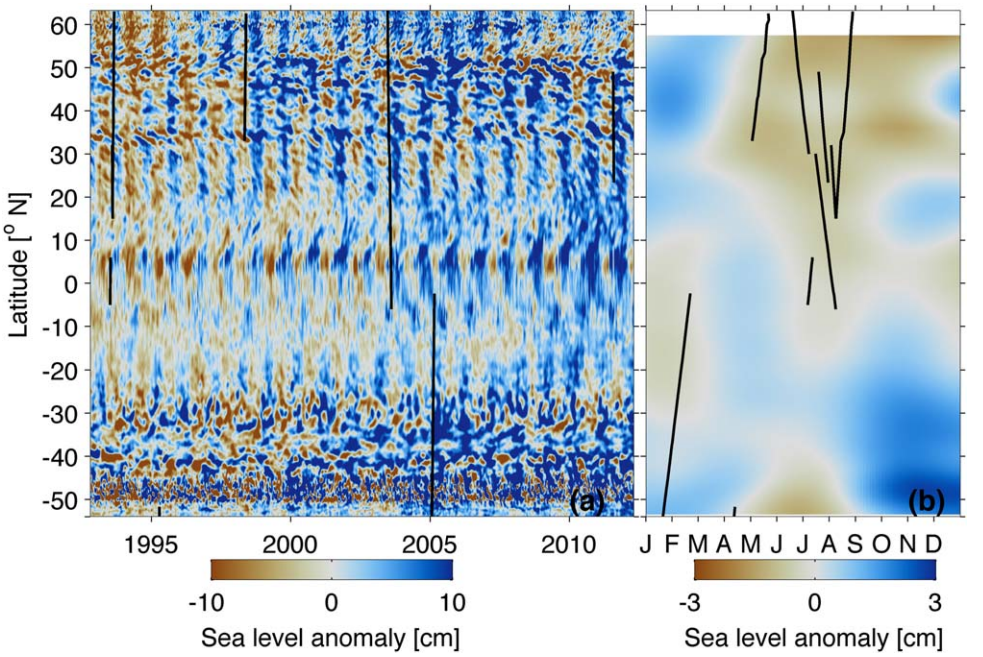

Figure 3. Total sea level variability from AVISO satellite altimetry (a) and seasonal mass cycle (January–December) from GRACE ocean bottom pressure (b) along approximately 25°W through the Atlantic Ocean. Full-depth in situ data are located along black lines.

3.1. Changes in Steric Height

We calculate local changes in SSL as trends between occupations along each section ($\partial SSL/\partial t$). Salinity (S) and potential temperature (θ) data along each section are gridded and interpolated onto an evenly spaced grid following *Purkey and Johnson* [2010]. The local $\partial SSL/\partial t$ owing to both thermostatic and halosteric contributions from the surface to the bottom between initial (i) and all subsequent occupations are calculated at each grid point along a section using

$$\partial SSL \Big/ \partial t = \frac{\int_{bottom}^{surface} \overline{\alpha}(z) \cdot (\theta(z) - \theta_i(z)) \cdot dz}{\partial t} + \frac{\int_{bottom}^{surface} \overline{-\beta}(z) \cdot (S(z) - S_i(z)) \cdot dz}{\partial t}. \quad (1)$$

The thermal expansion (α) and haline contraction (β) coefficients are calculated using the mean θ and S profile of the two occupations. The θ, S, α, and β profiles are interpolated from the 20 dbar pressure grid onto a 20 m depth grid and integrated using (1) from the surface to the bottom. The difference is converted into a rate per year by dividing by the difference in time between the two section occupations (∂t; e.g. Figure 4).

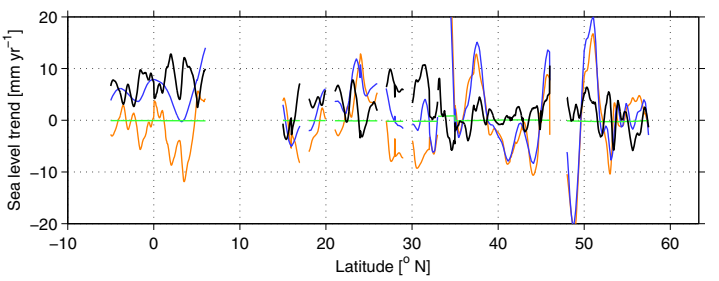

Figure 4. The rate of change in full-depth steric (orange) and mass seasonal cycle (green) contributions to total (blue) sea level trends (in mm yr^{-1}) between the 1993 and 2003 occupations of the section running along approximately 25°W through the Atlantic Ocean (Figure 1). The residual (black) of the total minus the sum of the full-depth steric and mass seasonal cycle is also shown.

3.2. Changes in SSH

We interpolate gridded Aviso SSH maps onto the hydrographic section locations in space and time. We apply a bilinear interpolant to each weekly mapped SSH to find the SSH anomaly along each section (e.g., Figure 3a). The SSH anomaly at each grid point along a section is linearly interpolated in time to the occupation dates (Figure 3a, black

lines). We calculate rates of change per year in SSH ($\partial SSH/\partial t$) along each section as the differences between the first occupation and each subsequent occupation divided by the elapsed times (e.g., Figure 4).

3.3. Seasonal Mass Corrections

We estimate offsets to correct for any local seasonal mass fluctuations between occupations ($\partial OM_{seasonal}/\partial t$) along sections using mapped GRACE OBP data. At each geographical grid point on the CSR 500 km smoothed maps, we fit a model with a mean value, linear trend, annual harmonic, and semiannual harmonic to the 10 year time series of monthly mass anomalies and find the standard error of each fit coefficient [*Wunsch*, 1996], accounting for temporal correlation of the residuals [*von Storch and Zwiers*, 1999]. At most locations, the annual cycle dominates, with mean and maximum amplitudes of 1.1 and 3.2 cm, respectively.

The mean, annual, and semiannual expected mass differences along each section between the initial and all subsequent occupations are calculated using the mean, annual, and semiannual coefficients found from the model fit at each location. We interpolate the model coefficients following the same methods used with the AVISO data (e.g., Figure 3b). The dates of occupations are used to calculate the expected seasonal changes in ocean mass ($\partial OM_{seasonal}/\partial t$) along each section (e.g., Figure 4). Most sections were occupied during similar seasons; therefore, the applied differences are usually only a fraction of the maximum annual and semiannual amplitudes (e.g., Figure 3b).

3.4. The Residual Method

We calculate mean trends in ocean mass and associated errors within seven regions (Figure 1). The residual trends between $\partial SSH/\partial t$ and $\partial SSL/\partial t$ plus $\partial OM_{seasonal}/\partial t$ along each section are calculated using:

$$res = {}^{\partial SSH}\big/_{\partial t} - {}^{\partial SSL}\big/_{\partial t} - {}^{\partial OM_{Seasonal}}\big/_{\partial t} \quad (2)$$

(Figure 4). We calculate the mean and variance of all residuals within each region (Table 1 and Figure 1) to estimate trends in ocean mass.

Each residual trend is a difference between an initial occupation (t_i) and second occupation (t_2). Within each region, the residual reflects the average time period of all section differences used. Therefore, we estimate the average trend period within each region as the mean t_i and mean t_2 of time of occupations (Table 1 and Figure 2).

We apply Student's t-test to find the two-tailed 90% confidence intervals from the standard deviation of the residuals within each region and combine them with the small uncertainty from the AVISO GIA correction (Table 1 and Figure 1). Degrees of freedom (DOF) are estimated from the sum of the length of all section divided by the typical global horizontal decorrelation length scale of the residual. A length scale of 156 km is used, which corresponds to the mean maximum of the integrals of spatially lagged autocovariances of all sections longer than 1000 km. Two-tailed 90% confidence limits assuming Student's t-distribution are calculated for each region. The GIA correction to the AVISO data set to account for changes in the seafloor introduces an additional $\pm$ 0.1 mm yr^{-1} uncertainty to the trend at the 90% confidence level. We combine this $\pm$ 0.1 mm yr^{-1} uncertainty with each of the regional variance-based uncertainties assuming the two terms are independent. Hence, we square the terms, sum them, and then take the square root. All error bars hereafter reflect these 90% confidence intervals.

Finally, we also calculate a global ocean mass trend using the area-weighted averages from each of the seven regional means. The ocean surface areas within each region, excluding the masked out areas within 300 km of land, are used to calculate a global-weighted summed mean and variance. Student's t-distribution is again used to estimate the 90% confidence interval around the mean using the weighted sum of regional variances and the sum of regional DOF, again taking the $\pm$ 0.1 mm yr^{-1} GIA correction uncertainty into account.

Throughout this paper, we combine variances with GIA uncertainties within each region to estimate 90% two-tailed confidence intervals, as discussed above. However, it is important to note here that there are also expected measurement uncertainties associated with each term in (2). Below we present a brief discussion of the expected measurement error from (2).

We estimate the measurement uncertainties associated with each of the instrumental or mapping terms ($\partial SSH/\partial t$, $\partial SSL/\partial t$, and $\partial OM_{seasonal}/\partial t$) from (2). The steric instrumental errors are estimated for each $\partial SSL/\partial t$ along every occupation by propagating the expected temperature and salinity CTD accuracies, 0.002°C and

Table 1. Regional and Global (Excepting the Arctic, North of 60°N) Trends in Sea Level Rise (SLR) Owing to Ocean Mass Addition Using the Residual Method (see Section 4) and the GRACE Method (see Section 5) Over the Time Periods Given With the Two-Tailed 90% Confidence Limits.

	Residual Method		GRACE Method	
Ocean Region	Mean Time Period of Trend (Year)	Mass Trend (mm yr^{-1})	Time Period of Trend (Year)	Mass Trend (mm yr^{-1})
North Pacific	1995.5–2006.8	1.53 ± 0.58	2003–2013	3.59 ± 0.71
North Atlantic	1996.2–2003.3	−0.09 ± 2.67	2003–2013	1.12 ± 0.89
South Pacific	1997.5–2008.1	1.03 ± 0.40	2003–2013	0.08 ± 0.62
South Atlantic	1993.5–2007.4	3.26 ± 1.41	2003–2013	3.23 ± 0.68
Pacific Sector of the Southern Ocean	1993.6–2006.7	−0.80 ± 1.23	2003–2013	−1.49 ± 1.18
Indian-Atlantic Sector of the Southern Ocean	1994.7–2001.8	4.66 ± 2.57	2003–2013	3.52 ± 0.61
Indian	1996.6–2005.5	1.12 ± 0.77	2003–2013	0.03 ± 0.55
Global Mean	1995.8–2006.3	1.47 ± 0.45	2003–2013	1.53 ± 0.36

0.002, respectively [*Joyce*, 1991], through (1). Therefore, this instrumental error is a function of sampling depth. The formal mapping errors from SSH maps, provided by AVISO, are interpolated onto each occupation following the same procedure discussed in section 2.2. The errors for $\partial SSH/\partial t$ between occupations are the sums of the squares of the mapped errors at each location along a section (e.g., Figure 4). We calculate the instrumental errors of $\partial OM_{seasonal}/\partial t$ in two ways. The mapped products used to model the seasonal cycle are estimated to have an error of 1–2 cm [*Chambers and Bonin*, 2012]. If we assume this mapping error is correct, we can calculate the weighted model coefficients and the model coefficient errors based on the known mapping error [*Wunsch*, 1996]. Alternatively, we can leave the measurement errors unknown and estimate the errors based on the variance of the residual from the model. Since the mapping errors are uniform for all months, the model coefficients are the same for either method.

Within each region, we calculate the average errors for $\partial SSH/\partial t$, $\partial SSL/\partial t$, and $\partial OM_{seasonal}/\partial t$ by dividing the means by the square roots of each variable's DOF. The DOF of the errors for $\partial SSL/\partial t$ are simply the numbers of total occupations within a region because biases in salinity or temperature tend to be instrument-specific and will therefore persist throughout each cruise, making each cruise only a single degree of freedom. The DOF of $\partial OM_{seasonal}/\partial t$ are determined by the map's smoothing length of 500 km divided by the length of sections in the region. The DOF of $\partial SSH/\partial t$, however, depends on the typical eddy decorrelation length scale, which varies between 10 and 500 km in the ocean, since the smoothing scale of AVISO is relatively small and generally captures these features. We find the mean long section length scale in the residual to be 156 km, which mostly reflects the variability from $\partial SSH/\partial t$ (e.g., Figure 4). Therefore, we chose a conservative length scale of 200 km as a "typical" eddy length scale to estimate the DOF of $\partial SSH/\partial t$.

The regional average uncertainties for $\partial SSH/\partial t$, $\partial SSL/\partial t$, and $\partial OM_{seasonal}/\partial t$ range between 0.04 to 0.46, 0.00 to 0.01, and 0.04 to 1.05 mm yr^{-1}, with global average uncertainties of 0.13, 0.01, and 0.20 mm yr^{-1}, respectively. While the sums of these errors are on the same order of magnitude as the regional mean variances, the error from the variances should capture most of these instrumental errors, assuming they are randomly distributed and not systematically biased in any way. In addition, errors may also arise from any internal ocean variability on time scales less than a week captured by $\partial SSL/\partial t$ but not $\partial SSH/\partial t$. However, here we consider large regional and global means to reduce the influence of high-frequency variability.

4. Ocean Mass Trends From GRACE

Global and regional trends in ocean mass gain are also calculated directly from the monthly regional mean OBP time series for the seven regions. A mean value, trend, annual harmonics, and semiannual harmonics are fit to the regional time series of water thickness equivalent using an unweighted model (Table 1). We retain the trends and trend errors and assume Student's t-distribution to estimate 90% confidence intervals (Figures 4 and 5; Table 1). We combine these uncertainties as discussed above with GIA correction uncertainties of 0.6 mm yr^{-1} in the North Atlantic and 0.3 mm yr^{-1} in all other regions. Again, a weighted global mean is calculated using the regional surface areas.

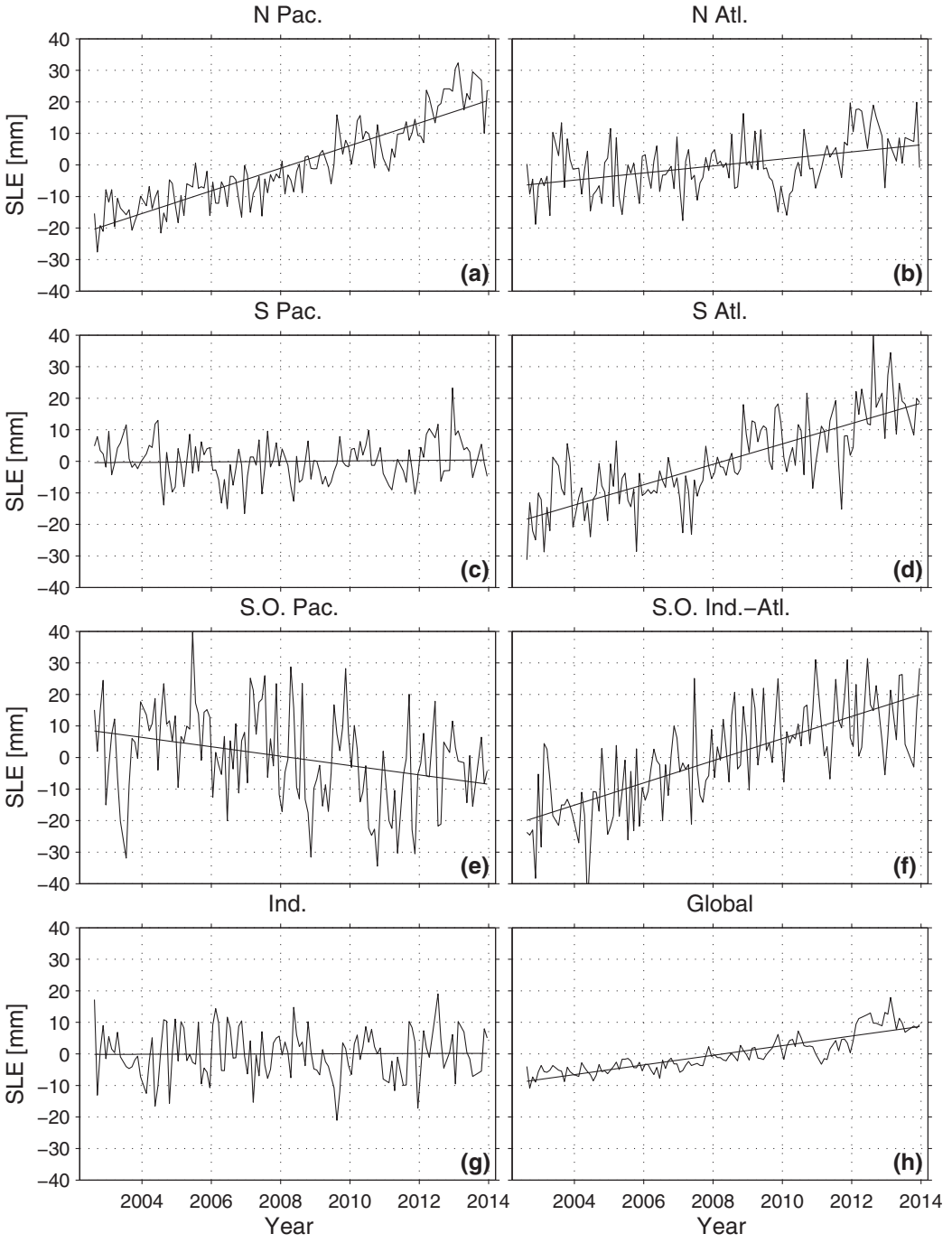

Figure 5. Linear trends (straight lines) of 2003–2013 time series of GRACE ocean bottom pressure anomaly with the annual and semi-annual seasonal cycle removed (squiggly lines) in Sea Level Equivalent (SLE) for the seven (a–g) regions (see Figure 1) and the area-weighted global mean (h).

We also calculate a weighted model fit [*Wunsch*, 1996] to evaluate if using the monthly standard errors of each time series, ranging from 0.6 to 2.7 cm of equivalent water thickness, produces significantly different error bars. This method produces 90% confidence intervals for the regional trends that are very similar to those found above. The weighted model errors are slightly larger than the unweighted errors except in the South and North Pacific where the errors of the monthly OBP are small and thus the weighted model errors are small. Furthermore, the global mean error for both methods agree within 0.03 mm yr^{-1}, well within error bars. We choose to discuss only the unweighted model errors combined with GIA correction uncertainties below.

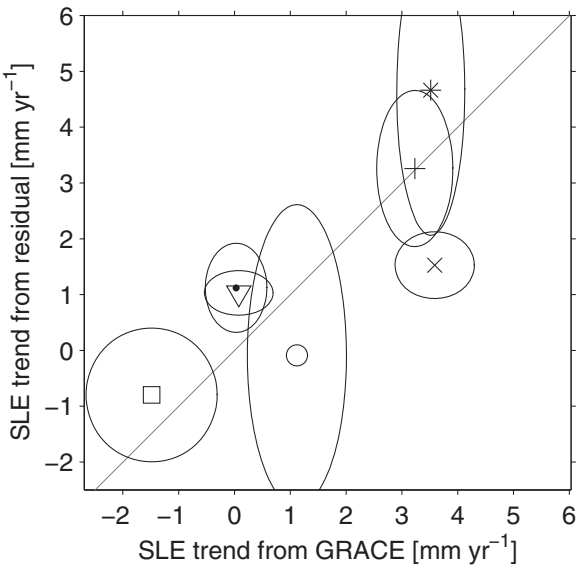

Figure 6. Regional mean ocean mass trends in the Indian (solid circle), North Atlantic (open circle), North Pacific (cross), South Atlantic (plus), Southern Ocean Atlantic-Indian sector (asterisk), Southern Ocean Pacific sector (square), and South Pacific (triangle) calculated from full-depth section residuals and from GRACE from 2003 to 2013 with 90% confidence intervals (Table 1) shown as error ellipses. Diagonal line indicates a one-to-one ratio.

5. Results

We find a global average ocean mass gain rate of 1.5 ($\pm$0.4) mm yr^{-1} SLR equivalent centered on 1996–2006 using the residual method and 1.5 ($\pm$0.4) mm yr^{-1} from 2003 to 2013 using the GRACE method, both with large regional variability (Figures 1 and 4; Table 1). The two methods' regional rates of ocean mass addition both reveal a consistent pattern and mostly agree with each other within error ellipses (Figure 6), despite covering different time periods. Both methods find regional differences in the magnitude of mass trends with 1–3 times greater rates in the North Pacific, South Atlantic, and the Atlantic-Indian sector of the Southern Ocean than in the Pacific sector of the Southern Ocean or North Atlantic regions (Figures 1, 5, and 6). These regional differences from the global mean ocean mass trend are consistent with previous ocean mass regional studies [e.g., *Johnson and Chambers*, 2013; *Bamber and Riva*, 2010] and suggest changes in wind stress curl have driven higher than average trends of ocean mass addition in the North Pacific and Atlantic-Indian sector of the Southern Ocean while changes in the Earth's gravitational field have driven lower than average trends near West Antarctica and Greenland, where the largest land ice losses has occurred.

The residual method ocean mass trends vary regionally from -0.8 ($\pm$1.2) mm yr^{-1} in the Pacific sector of the Southern Ocean to $+4.7$ ($\pm$2.6) mm yr^{-1} in the Indian-Atlantic sector of the Southern Ocean (Figure 1; Table 1). Five of the seven regions have statistically significant positive trends. The North Atlantic and Pacific sectors of the Southern Ocean both have negative mass trends, albeit not statistically significantly different from zero. Each regional rate reflects a slightly different time period based on when the sections were occupied within the region (Figure 2). The mean initial occupation (t_i) is between 1993 and 1997 for all regions. The mean second occupation (t_2) ranges from 2001 to 2008, with trends over a time span of 10.3 years on average (Table 1 and Figure 2).

The model fits to the regional monthly mass anomalies from the GRACE method also do a good job of capturing low-frequency variability in the South Atlantic, North Pacific, and Atlantic-Indian sector of the Southern Ocean, all showing large, statistically significant positive mass trends of 3.2 ($\pm$0.7), 3.6 ($\pm$0.7), and 3.5 ($\pm$0.6) mm yr^{-1}, respectively (Figures 5a, 5d, and 5f). The North Atlantic has a small, but statistically significant, trend of 1.1 ($\pm$0.9) mm yr^{-1}, albeit with larger errors on the monthly means and including areas with potential land mass leakages from ice loss (Figure 5b) [e.g., *Chambers*, 2009]. Both the model fits to the Indian and South Pacific regions capture the large mass seasonal cycle but have no significant decadal trend (Figures 5c and 5g).

The Pacific sector of the Southern Ocean and the North Pacific are the only regions where the model applied to the GRACE data has residuals with structure. The North Pacific region has residual structure that increases by $\sim$1 cm from 2003 to 2007 and then returns to zero afterward (Figure 5a). This result is consistent with large, low-frequency fluctuations in bottom pressure throughout the subpolar gyre observed over this period [*Chambers*, 2011, Figure 6]. In the Pacific sector of the Southern Ocean, the amplitude of the model residual is as large as the model, so the model does not fit the data well. The model does find a slight negative trend of -1.5 ($\pm$1.2) mm yr^{-1}; however, this trend is not consistent over the entire time period and subsampling yields radically different trends (Figure 5e). The proximity of this region to West Antarctic ice sheets, with their large mass losses, may introduce short timescale noise and systematic biases in the

trend. Even with the 300 km land mask and applied corrections, land leakage from areas with large changes can still introduce large bias errors [*Chambers*, 2009].

5.1. Regional Trends

Observed local deviations from the global mean ocean mass trend likely reflect changes in either surface-forced wind stress curl or changes in Earth's gravitational field and rotation from land ice mass changes. Here both methods have already corrected for the GIA, therefore, it is not expected to be driving the observed variability outside the stated errors. Independently, both methods suggest the Indian-Atlantic sector of the Southern Ocean, South Atlantic, and North Pacific are gaining mass while the Pacific sector of the Southern Ocean is losing mass, despite estimating trends over different, although overlapping, time periods (Figures 1 and 5). The regional mean mass trends and 90% confidence intervals are discussed in light of previous work and forcing mechanisms.

Consistent with expected ocean mass sea level changes from the large ice mass loss off West Antarctic and Greenland, the residual method finds lower than global average mass trends in the North Atlantic and the Pacific sector of the Southern Ocean. Changes in Earth's gravitational field and rotation from the combined mass loss for Greenland, West Antarctica, Alaska, and glaciers will decrease relative sea level on the order of -1 mm yr^{-1} around West Antarctica, Greenland, and Alaska, with a positive relative SLR between 20°N and 40°S [*Bamber and Riva*, 2010]. Here we find a large mass loss of -0.8 (± 1.2) mm yr^{-1} between 1993 and 2006 from the residual method and -1.5 ($\pm$ 1.2) between 2003 and 2013 from the GRACE method in the Pacific sector of the Southern Ocean. This negative trend has been previously noted using GRACE products and credited to land leakage from the melting of the West Antarctic Ice Sheet [*Chambers*, 2009]. However, here we find a consistent negative trend using the residual method, independent from the GRACE method, suggesting the mass loss signal could in part be capturing real decreases in ocean mass in this region.

The second region of expected negative ocean mass sea level anomaly from gravitational effects is in the North Atlantic, owing to Greenland's large ice melt rate of 166 Gt yr^{-1}. Here, the residual method finds a negative mass loss rate of -0.1 ($\pm$ 2.7) mm yr^{-1} between 1996 and 2003 with the very large error reflecting large regional variability between occupations. The GRACE method, however, finds a positive, but still less than the global mean, ocean mass trend of 1.1 ($\pm$0.9) mm yr^{-1} (Figure 5b). The difference of the means between the two methods is consistent within uncertainty estimates but could also reflect interdecadal variability causing a different rate of mass gain over the different time periods covered by the two methods.

The residual and GRACE methods both find relatively high rates of mass addition in the South Atlantic and Southern Ocean sector of the Atlantic, most likely reflecting regional changes in winds. The residual method shows the Indo-Atlantic sector increasing mass at a rate of 4.7 ($\pm$2.6) mm yr^{-1} from 1994 to 2001 (Figures 1 and 4f; Table 1). The residual method agrees well with the GRACE method mean of 3.5 ($\pm$0.6) mm yr^{-1} found here (Figure 5f and Table 1) and local GRACE OBP trends as high as 2–5 mm yr^{-1} above the global mean rate in these regions reported by *Johnson and Chambers* [2013]. They suggest these changes could be linked to small variations in the strength of the Antarctic Circumpolar Current [e.g., *Hogg et al*., 2014] or the Weddell Gyre. In the South Atlantic, the residual method estimates a mass increase of 3.3 ($\pm$1.4) mm yr^{-1}, which, while based on limited data (Figure 1), is consistent with the estimate from the GRACE methods of 3.2 ($\pm$0.7) mm yr^{-1}. Again, here both methods agree with the basin-wide anomalies high rate of ocean mass addition found by *Johnson and Chambers* [2013] from the GRACE mapped product. The mass gain estimated by both methods are higher than expected from the global mean plus gravitational and rotational effects in this region, suggesting overlying wind patterns have shifted in this region and indicating a topic for further analysis.

Both methods yield an above average ocean mass gain in the North Pacific, consistent with the well-documented local changes in the strength of wind stress in the northwest side of that basin [*Chambers and Willis*, 2008; *Chambers*, 2011; *Cheng et al*., 2013]. The residual method finds a positive ocean mass trend of 1.5 ($\pm$0.6) mm yr^{-1} gain from 1995 to 2006, albeit half the magnitude of the GRACE method rate of 3.6 ($\pm$0.7) mm yr^{-1} from 2003 to 2013 (Figures 1 and 4a; Table 1).

Finally, the residual and GRACE methods find somewhat inconsistent mass rates in the South Pacific and Indian regions (Table 1; Figures 1 and 6). The rates of mass gain from the residual method is $\sim$1 mm yr^{-1} in both regions, within error of the global mean mass rate, hence suggesting no dynamical change from

wind-driven circulation. However, the GRACE method finds no mass gain in either basin, suggesting a negative dynamical response counteracting the global mean positive ocean mass addition trend and positive sea level effects from changes in the gravitational field. In the Indian basin, however, the December 2004 Indonesia earthquake could affect GRACE products in this region [e.g., *Chen et al*., 2007], or there may be interdecadal variability, with rate of mass gain changing over the somewhat different time periods considered by the two methods.

5.2. Global Trends

The residual and GRACE methods both find the area-weighted global mean mass contribution to SLR to be 1.5 ($\pm$0.4) mm yr^{-1}, over 1996–2006 for the residual method and 2003–2013 for the GRACE method (Figure 5h and Table 1). Neither global mean includes the Arctic and both are area-weighted means of the seven regions. The 90% confidence intervals from the two methods are similar, despite reflecting different uncertainties. The residual method's confidence interval primarily reflects the large variance in the residual, with only a small contribution from the GIA correction uncertainty. In contrast, the GRACE method sees a relatively small variance in the trend (Figure 1h) but the error is increased substantially by the 0.3 mm yr^{-1} GIA correction uncertainty, inflating the total uncertainty to 0.4 mm yr^{-1}.

The two methods are in very good agreement with each other and previous estimates. The residual method 1996–2006 trend is within error of *Church et al*. [2011] 1993–2008 total mass contribution of 1.66 ($\pm$0.46) mm yr^{-1}. Our GRACE method global mean is slightly less than *Johnson and Chambers* [2013] estimate of 1.8 mm yr^{-1} over a very similar period, but theirs is a global averaging kernel and our weighted sum of smaller areas both attenuates the trend slightly and excludes the Arctic.

5.3. The $\partial OM_{seasonal}/\partial t$ Term

Seasonal mass redistribution adjustments, the $\partial OM_{seasonal}/\partial t$ term in (2), are a small contribution to the SLR budget in all regions, owing to both the comparatively small seasonal cycle and because most repeat sections are occupied during similar months (e.g., Figures 2b and 3). To demonstrate this, we recalculate regional residuals from the residual method using two variations on $\partial OM_{seasonal}/\partial t$. First, the regional means are recalculated using the coefficients from JPL and GFZ instead of CSR. The GFZ coefficients are slightly different from JPL or CSR; however, these variations do not affect the regional or global trends. Second, if the $\partial OM_{seasonal}/\partial t$ term is excluded from (2) altogether, the regional trends stay within the 90% confidence intervals in all except the South Pacific region, where the regional trend decreases substantially from 1.0 ($\pm$0.4) mm yr^{-1} with the $\partial OM_{seasonal}/\partial t$ term to 0.3 ($\pm$0.4) mm yr^{-1} without the $\partial OM_{seasonal}/\partial t$ term. The global mean estimate is insensitive to which GRACE mapped products are used and, when no GRACE seasonal adjustments are used, only changes slightly, to 1.4 $\pm$ 0.5 mm yr^{-1}.

Applying the $\partial OM_{seasonal}/\partial t$ offset in (2) limits our study area to regions of the ocean farther than 300 km from the coast owing to the land leakage mask associated with the GRACE mapped products. We test the effect of this mask on our results by calculating the regional residual from (2) without GRACE, both with the land mask and without. The land mask eliminates a substantial fraction of our section data, changing the total length of all sections used from 1.4×10^5 km to 1.1×10^5 km. Nonetheless, the only regions whose rates change $>$ 0.1 mm yr^{-1} is the Indian-Atlantic sector of the Southern Ocean and the Indian Ocean, which increased by 0.7 and 0.6 mm yr^{-1}, respectively. Again, the global trends are essentially unaffected by the masking, with the rates increasing by $\sim$ 0.1 mm yr^{-1}, well within the error bars.

6. Deep Steric Contributions

We evaluate the relative importance of the deep steric contribution to the SLR budget by using a variation of the residual method. Here we are asking, "How much error is introduced into the SLR budget when the full water-column steric contribution is not included?". We do not directly calculate the steric component here because the temporal and spatial coverage of the data used is not sufficient to capture the high variability in the upper water column. However, by taking the residual between SSH and the upper water column steric contribution, we remove most of this variability, and are left with the mass plus the deep steric contribution. Therefore, we calculate the regional and global ocean mass addition trends by integrating (1) from the surface to 300, 700, 1000, 2000, 3000, and 4000 m and compare the results to the ocean mass addition trends found using the full water-column steric contribution.

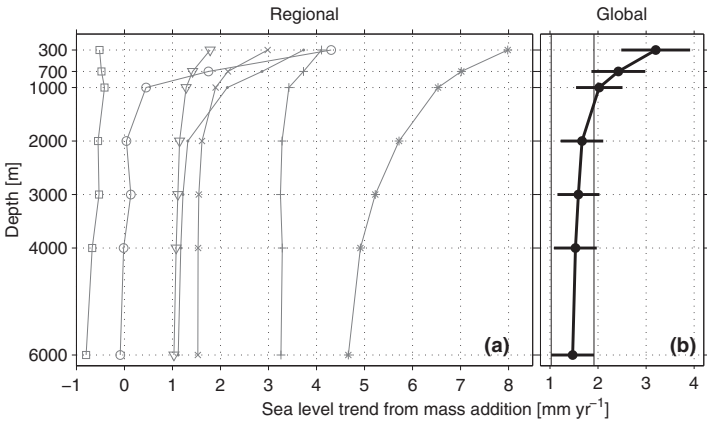

Figure 7. Area-average trends of residuals between total sea level and steric contributions in (a) the Indian (solid circles), North Atlantic (open circles), North Pacific (crosses), South Atlantic (pluses), Southern Ocean Atlantic-Indian sector (asterisks), Southern Ocean Pacific sector (squares), and South Pacific (triangles) and (b) the global average with 90% confidence intervals versus depth of integration from the surface. The 6000 m 90% confidence interval is extended over all depths for comparison (vertical lines).

The deep ocean steric contribution is found to add 0.78, 0.40, 0.36, 0.07, 0.06, and 0.05 mm yr^{-1} from 300–700, 700–1000, 1000–2000, 2000–3000, 3000–4000, and 4000–6000 m, respectively. Therefore, neglecting the deep SSL component below 300, 700, 1000, or 2000 m increases the expected mass component of the SLR budget by 117%, 65%, 38%, or 13%, respectively (Figure 7). The sparse sampling of full-depth repeat sections may lead to aliasing of steric variability, captured in SSH but not SSL when the full-column steric term is not used in (2). The large, deep steric contribution estimated here between 300 and 2000 m of 1.53 mm yr^{-1}, over twice as large as previously estimated rates [e.g., *Levitus et al*., 2012], most likely reflects a sampling bias. However, this calculation suggests that previous sea level budgets calculating mass addition from the difference between total sea level and upper steric contributions, neglecting say the ocean below 2000 m, where aliasing is likely smaller, may overestimate that mass contribution by 13%. This result is consistent with previous studies estimating that the deep steric expansion below 2000 m is contributing roughly 6% to the total SLR budget [e.g., *Purkey and Johnson*, 2010]. Finally, if the steric contribution is limited to only the upper 1000 m or less of the water column, the residual no longer falls within the 90% confidence limits of the GRACE method, and the budget will not close (Figure 7).

The relative contribution of the deep ocean to the SLR budget varies considerably by region (Figure 7). In regions where deep convection communicates surface heating to the deep ocean, one would expect a higher contribution from deep steric changes. Accordingly, the Indian-Atlantic sector of the Southern Ocean has substantial contributions through the water column, extending below 4000 m. The North Atlantic also has a large contribution from steric changes from 700 to 2000 m. In the Pacific sector of the Southern Ocean, however, there was no contribution between 300 and 6000 m outside the error bars, inconsistent with previous deep steric estimates in the region, possibly owing to less data used in this region because of the 300 km land mask and the post-1992 repeat criteria used here (e.g., Figure 1 versus Figure 1 of *Purkey and Johnson* [2010]). Elsewhere, the deep ocean below 2000 m contributes 1–17% to the residual ocean mass calculation, roughly consistent with previous deep steric contributions from deep ocean warming [e.g., *Purkey and Johnson*, 2010].

7. Discussion

The analysis from the residual method presented here captures long-term large-scale trends in sea level owing to mass addition between the mid-1990s and mid-2000s. Given the limited temporal coverage, a linear trend is all that can be resolved. However, we find a linear trend is a good model of ocean mass from 2003 to 2013 from the GRACE method in most of the seven regions (Figure 5) and the AVISO SSH record is also well described by a linear trend in SSH over the whole time period considered here [*Church et al*., 2013]. Furthermore, we find agreement within the 90% confidence intervals of the two methods globally and regionally in many cases, suggesting the global trend rate from 1996 to 2006 versus 2003 to 2013 has not changed significantly, or at least not outside our error estimates (Figure 6).

However, there is certainly interannual [*Boening et al*., 2012; *Fasullo et al*., 2013, *Cazenave et al*., 2014] and spatial [e.g. *Johnson and Chambers*, 2013] variability in the ocean mass that is not captured in our analysis (Figure 5). The 90% confidence intervals reported should account for both spatial and

temporal variability, assuming the data falls randomly in time to avoid any systematic temporal biases and are evenly distributed across each region to avoid spatial biases (Figures 1 and 2). These two assumptions are discussed below.

First, we assume the temporal resolution of our section differences is sufficient to capture the average trend. The differences in times of the initial occupation of the sections (Figure 2; red) and each subsequent reoccupation (Figure 2; blue) are reasonably random and should not lead to temporal biases. Again, the long-term mass trend has mostly been linear over the time period studied, with the exception of the strong El Nino Southern Oscillation (ENSO) events in 1998 and 2011 [e.g., *Cazenave et al*., 2014]. Only the North and South Atlantic have a high percentage of data during either of these large ENSO events, which could slightly bias the estimates in these two regions.

Second, we balance making our regions small enough to capture regional variability in ocean mass but large enough so the regional means rise above the noise. The variability at any given location along the sections is 10 times the amplitude of the regional ocean mass trends presented here and therefore, at any given point the residual is meaningless (e.g., Figure 4). However, the residuals averaged over large enough regions should reflect the large-scale mass signal, estimated within the stated errors.

Each region has good spatial coverage with the exception of the North Pacific, South Atlantic, and Indian oceans. The North Pacific region has more data in the west than east, possibly biasing the residual estimate high. The Indian Ocean is missing data in the north, and therefore, the result may more accurately reflect changes south of the equator. Finally, the South Atlantic regional trend is based primarily on three occupation of one section at 30°S. However, the along-section trends from the different occupations are similar and the 2003–2012 mass trend is fairly uniform across the region [*Johnson and Chambers*, 2013].

In summary, here we present a new estimate of ocean mass addition using data as early as October 1992, calculated independently of GRACE, and using a full-column steric SLR budget. This GRACE-independent residual method finds a global mass addition trend of 1.5 ($\pm$0.4) mm yr^{-1} from 1996 to 2006 by calculating the difference between total SSH and in situ full-depth SSL. This finding is in good agreement with the global ocean mass trend of 1.5 ($\pm$0.4) mm yr^{-1} from 2003 to 2013 found using GRACE data directly. Both methods agree on large-scale patterns of higher rates of ocean mass gain in the Indian-Atlantic sector of the Southern Ocean, the North Pacific, and the South Atlantic. Finally, we have also estimated the relative importance of the deep ocean to the SLR budget, with the deep ocean steric expansion below 700 m equivalent to 65% of the ocean mass contribution to sea level, and 13% below 2000 m.

This work highlights the importance of the deep ocean contribution to the global SLR budget. In order to accurately assess past and future local and global trends in SLR, it is necessary to monitor the deep ocean steric changes through full-depth profiling floats, deep gliders, and the continuation of high-quality full-depth ship-based data such as those taken under the auspices of GO-SHIP.

Acknowledgments

The altimeter products used here are available at http://www.aviso.oceanobs.com/en/data.html and were downloaded in July 2013. They were produced by Ssalto/*Duacs* and distributed by *AVISO*, with support from *CNES* (http://www.aviso.oceanobs.com/duacs/). GRACE ocean data were processed by Don P. Chambers, supported by the NASA MEASURES Program and are available at http://GRACE.jpl.nasa.gov and were downloaded in May 2013. The in situ ocean data from the WOCE, CLIVAR, and GO-SHIP Programs used here are available at http://cchdo.ucsd.udu and were downloaded in September 2013. Comments from Cecilia Bitz, Susan Hautala, Mark Warner, and two anonymous reviewers greatly improved this manuscript. The findings and conclusions in this article are those of the authors and do not necessarily reflect the views of the National Oceanic and Atmospheric Administration (NOAA). This work was supported by the NOAA Climate Program Office, NOAA Research, and NASA Headquarters under the NASA Earth and Space Fellowship Program—Grant NNX11AL89H. DPC was funded through NASA Grant NNX12AL28G. PMEL Contribution 4170.

References

Ablain, M., A. Cazenave, G. Valladeau, and S. Cuinehut (2009), A new assessment of the error budget of global mean sea level rate estimated by satellite altimetry over 1993–2008, *Ocean Sci.*, *5*, 193–201, doi:10.5194/os-5-193-2009.

Bamber, J., and R. Riva (2010), The sea level fingerprint of recent ice mass fluxes, *Cryosphere*, *4*, 621–627, doi:10.5194/tc-4-621-2010.

Boening, C., J. K. Willis, F. W. Landerer, R. S. Nerem, and J. Fasullo (2012), The 2011 La Niña: So strong, the oceans fell, *Geophys. Res. Lett.*, *39*, L19602, doi:10.1029/2012GL053055.

Cazenave, A., K. Dominh, S. Guinehut, E. Berthier, W. Llovel, G. Ramillien, M. Ablain, and G. Larnicol (2009), Sea level budget over 2003–2008: A reevaluation from GRACE space gravimetry, satellite altimetry and Argo, *Global Planet. Change*, *65*, 83–88, doi:10.1016/j.gloplacha.2008.10.004.

Cazenave, A., H. B. Dieng, B. Meyssignac, K. von Schuckmann, B. Decharme, and E. Berthier (2014). The rate of sea-level rise., *Nat. Clim. Change*, *4*(5), 358–361, doi:10.1038/nclimate2159.

Chambers, D. P. (2009), Calculating trends from GRACE in the presence of large changes in continental ice storage and ocean mass, *Geophys. J. Int.*, *176*, 415–419, doi:10.1111/j.1365-246X.2008.04012.x.

Chambers, D. P. (2011), ENSO-correlated fluctuations in ocean bottom pressure and wind-stress curl in the North Pacific, *Ocean Sci.*, *7*, 685–692, doi:10.5194/os-7-685-2011.

Chambers, D. P., and J. A. Bonin (2012), Evaluation of Release-05 GRACE time-variable gravity coefficients over the ocean, *Ocean Sci.*, *8*, 859–868, doi:10.5194/os-8-859-2012.

Chambers, D. P., and J. K. Willis (2008), Analysis of large-scale ocean bottom pressure variability in the North Pacific, *J. Geophys. Res.*, *113*, C11003, doi:10.1029/2008JC004930.

Chambers, D. P., and J. K. Willis (2010), A global evaluation of ocean bottom pressure from GRACE, OMCT, and steric-corrected altimetry, *J. Atmos. Oceanic Tech.*, *27*, 1–8, doi:10.1175/2010JTECHO738.1.

Chambers, D. P., J. Wahr, M. E. Tamisiea, and R. S. Nerem (2010), Ocean mass from GRACE and glacial isostatic adjustment, *J. Geophys. Res.*, *115*, B11415, doi:10.1029/2010JB007530.
Chen, J. L., C. R. Wilson, B. D. Tapley, and S. Gran (2007), GRACE detects coseismic and postseismic deformation from the Sumatra-Andaman earthquake, *Geophys. Res. Lett.*, *34*, L13302, doi:10.1029/2007GL030356.
Cheng, X., L. Li, Y. Du, J. Wang, and R.-X. Huang (2013), Mass-induced sea level change in the northwestern North Pacific and its contribution to total sea level change, *Geophys. Res. Lett.*, *40*, 3975–3980, doi:10.1002/grl.50748.
Church, J. A., and N. J. White (2011), Sea-level rise from the late 19th to the early 21st century, *Surv. Geophys.*, *32*, 585–602, doi:10.1007/s10712-011-9119-1.
Church, J. A., et al., (2013), Sea level change, in *Climate Change 2013: The Physical Science Basis. Contribution of Working Group I to the Fifth Assessment Report of the Intergovernmental Panel on Climate Change*, edited by T. F. Stocker et al., Cambridge Univ. Press, Cambridge, U. K., doi:10.1017/CBO9781107415324.026.
Church, J. A., N. J. White, L. F. Konikow, C. M. Domingues, J. G. Cogley, E. Rignot, J. M. Gregory, M. R. van den Broeke, A. J. Monaghan, and I. Velicogna (2011), Revisiting the Earth's sea-level and energy budgets from 1961 to 2008, *Geophys. Res. Lett.*, *38*, L18601, doi:10.1029/2011GL048794.
Domingues, C. M., J. A. Church, N. J. White, P. J. Gleckler, S. E. Wijffels, P. M. Barker, and J. R. Dunn (2008), Improved estimates of upper-ocean warming and multi-decadal sea-level rise, *Nature*, *453*, 1090–1093, doi:10.1038/nature07080.
Ducet, N., P.-Y. Le Traon, and G. Reverdin (2000), Global high-resolution mapping of ocean circulation from TOPEX/Poseidon and ERS-1 and −2, *J. Geophys. Res.*, *105*, 19,477–19,498.
Fasullo, J. T., C. Boening, F. W. Landerer, and R. S. Nerem (2013), Australia's unique influence on global sea level in 2010–2011, *Geophys. Res. Lett.*, *40*, 4368–4373, doi:10.1002/grl.50834.
Flechtner, F. (2007), AOD1B Product Description Document for Product Releases 01 to 04, *Rep. GRACE 327–750*, 43 pp., Univ. of Tex. at Austin.
Fukumori, I., and O. Wang (2013), Origins of heat and freshwater anomalies underlying regional decadal sea level trends, *Geophys. Res. Lett.*, *40*, 563–567, doi:10.1002/grl.50164.
Hogg, A. McC., M. P. Meredith, D. P. Chambers, E. P. Abrahamsen, C. W. Hughes, and A. K. Morrison (2014), Recent trends in the Southern Ocean eddy field and Antarctic Circumpolar Current, *Geophys. Res. Lett.*, in press.
Johnson, G. C., and D. P. Chambers (2013), Ocean bottom pressure seasonal cycles and decadal trends from GRACE Release-05: Ocean circulation implications, *J. Geophys. Res. Oceans*, *118*, 4228–4240, doi:10.1002/jgrc.20307.
Joyce, T. M. (1991), Introduction to the Collection of Expert Reports Compiled for the WHP Program, WOCE Hydrographic operations and methods. WOCE Operations Manual, *WHP Off. Rep. WHPO-91-1*, *WOCE Rep. 68/91*, WOCE Hydrographic Program Off., Woods Hole, Mass.
LeBel, D. A., et al. (2008), The formation rate of North Atlantic deep water and eighteen degree water calculated from CFC-11 inventories observed during WOCE, *Deep Sea Res., Part I*, *55*, 891–910.
Leuliette, E., and J. Willis (2011), Balancing the sea level budget, *Oceanography*, *24*, 122–129, doi:10.5670/oceanog.2011.32.
Leuliette, E. W., and L. Miller (2009), Closing the sea level rise budget with altimetry, Argo, and GRACE. *Geophys. Res. Lett.*, *36*, L04608, doi:10.1029/2008GL036010.
Leuliette, E. W., R. S. Nerem, and G. T. Mitchum (2004), Calibration of TOPEX/Poseidon and Jason Altimeter data to construct a continuous record of mean sea level change, *Mar. Geod.*, *27*, 79–94, doi:10.1080/01490410490465193.
Levitus, S., et al. (2012), World ocean heat content and thermosteric sea level change (0–2000 m), 1955–2010, *Geophys. Res. Lett.*, *39*, L10603, doi:10.1029/2012GL051106.
Lombard, A., A. Cazenave, K. DoMinh, C. Cabanes, and R. S. Nerem (2005), Thermosteric sea level rise for the past 50 years; comparison with tide gauges and inference on water mass contribution, *Global Planet. Change*, *48*, 303–312.
Lorbacher, K., S. J. Marsland, J. A. Church, S. M. Griffies, and D. Stammer (2012), Rapid barotropic sea level rise from ice sheet melting, *J. Geophys. Res.*, *117*, C06003, doi:10.1029/2011JC007733.
Lowe, J. A., and J. M. Gregory (2006), Understanding projections of sea level rise in a Hadley Centre coupled climate model, *J. Geophys. Res.*, *111*, C11014, doi:10.1029/2005JC003421.
Mauritzen, C., A. Melsom, and R. T. Sutton (2012), Importance of density-compensated temperature change for deep North Atlantic Ocean heat uptake, *Nat. Geosci.*, *5*, 905–910, doi:10.1038/ngeo1639.
Merrifield, M. A., P. R. Thompson, M. Lander, and K. Aagaard (2012), Multidecadal sea level anomalies and trends in the western tropical Pacific, *Geophys. Res. Lett.*, *39*, L13602, doi:10.1029/2012GL052032.
Nerem, R. S., D. P. Chambers, C. Choe, and G. T. Mitchum (2010), Estimating mean sea level change from the TOPEX and jason altimeter missions, *Mar. Geod.*, *33*, 435–446, doi:10.1080/01490419.2010.491031.
Orsi, A. H., G. C. Johnson, and J. L. Bullister (1999), Circulation, mixing, and production of Antarctic Bottom Water, *Prog. Oceanogr.*, *43*, 55–109, doi:10.1016/S0079-6611(99)00004-X.
Purkey, S. G., and G. C. Johnson (2010), Warming of global Abyssal and deep southern ocean waters between the 1990s and 2000s: Contributions to global heat and sea level rise budgets, *J. Clim.*, *23*, 6336–6351, doi:10.1175/2010JCLI3682.1.
Rhein, M., et al. (2013), Observations: Ocean, in *Climate Change 2013: The Physical Science Basis. Contribution of Working Group I to the Fifth Assessment Report of the Intergovernmental Panel on Climate Change*, edited by T. F. Stocker et al., Cambridge Univ. Press, Cambridge, U. K., doi:10.1017/CBO9781107415324.010.
Stammer, D., A. Cazenave, R. M. Ponte, and M. E. Tamisiea (2013), Causes for contemporary regional sea level changes, *Annu. Rev. Mar. Sci.*, *5*, 21–46, doi:10.1146/annurev-marine-121211-172406.
von Schuckmann, K., J.-B. Sallée, D. Chambers, P.-Y. Le Traon, C. Cabanes, F. Gaillard, S. Speich, and M. Hamon (2014), Consistency of the current global ocean observing systems from an Argo perspective, *Ocean Sci.*, *10*, 547–557, doi:10.5194/os-10-547-2014.
von Storch, H. and F. W. Zwiers (1999), *Statistical Analysis in Climate Research*, 484 pp., Cambridge Univ. Press, Cambridge, Mass.
Willis, J. K., D. P. Chambers, and R. S. Nerem (2008), Assessing the globally averaged sea level budget on seasonal to interannual timescales, *J. Geophys. Res.*, *113*, C06015, doi:10.1029/2007JC004517.
Wunsch, C. (1996), *The Ocean Circulation Inverse Problem*, 458 pp., Cambridge Univ. Press, Cambridge, Mass.